https://doi.org/10.1016/j.jdent.2020.103402

Title: Characterisation of mineral loss as a function of depth using confocal laser scanning microscopy to study erosive lesions in enamel: A novel non-destructive image processing model.

Keywords: Erosion, Confocal, Porosity, Enamel

Authors: Mathew J. F. Hookham[1*], Richard J.M. Lynch[2], Declan P. Naughton[1]

[1] School of Life Sciences, Pharmacy and Chemistry, Kingston University London, United Kingdom

[2] Oral Healthcare, Glaxo-Smith Kline, Weybridge, United Kingdom

[*]Corresponding Author

Mathew James Frederick Hookham

School of Life Sciences, Pharmacy and Chemistry

Kingston University London

Penrhyn Rd,

Kingston upon Thames, Surrey, KT1 2EE, United Kingdom

Tel: (+44)7427493577

E-Mail: K1112053@kingston.ac.uk

Key Words: Erosion, Confocal, Porosity, Citric-Acid, Enamel

Abstract:

Objective: The aim was to develop a novel image processing protocol for confocal laser scanning microscopy (CLSM) to study mineral distribution within erosive lesions as a function of depth.

Methods: Polished bovine enamel samples (n=80) were divided into groups (8/group) with similar mean surface microhardness (SMH) values. Samples underwent erosion (1% citric acid pH3.8) for 1,5,10,15, or 30min, with or without stirring giving 10 treatment groups in a 2*5 factorial design. SMH was used to measure erosive softening. Profilometry was used to measure bulk tissue loss. Samples were then stained with rhodamine-B (0.1mM, 24h) and imaged using CLSM. Image processing was used to measure fluorescence volume (FV) as a function of depth for each image. The data from reference images were subtracted from post-erosive data to determine changes in fluorescent volume (ΔFV) as a function of depth. 2-way ANOVA and linear regression analysis were used where applicable.

Results: Surface softening and bulk tissue loss increased with acid erosion duration with or without stirring. Stirring significantly increased net softening at each time point; specimens underwent significantly more bulk tissue loss ($P<0.05$). CLSM showed the erosive lesion deepened as exposure to acid increased, and that at the near surface (0-10μm) FV and ΔFV increased rapidly for stirred solutions. The increase in pore space translated to a softer surface as measured by SMH.

Conclusion: This novel non-destructive method allows concurrent quantification of dental erosion by mineral loss as a function of depth, and qualitative characterisation of microstructural changes during early erosion.

1 Introduction

The Increasing prevalence of dental erosion, especially in adolescents, largely reflects frequent exposure to dietary acids (e.g citric acid) [1–3]. Dental erosion, typically considered a surface phenomenon, is caused by direct acid contact with the enamel surface. This contrasts to caries subsurface lesions, formed through bacterial fermentation of sugars and starch into acid within the plaque biofilm, where the surface can remain largely intact until cavitation occurs [4]. Other distinct differences are the shallow erosive lesion, and source of acid being extrinsic (environmental or dietary) or intrinsic (gastric) [5–7]. The lack of a bacterial biofilm allows for rapid surface demineralisation by the acid, creating the characteristic surface softened zone of an erosive lesion [7]. Progression of erosion occurs through removal of bulk tissue from the surface, meaning much of the literature is focused on the effect to the surface, such as hardness and bulk tissue loss, ignoring any potential subsurface changes [8,9]. One major reason for this lack of subsurface information is the limited number of suitable methods capable of measuring these changes, owing to the shallow and fragile nature of erosive lesions.

Techniques such as transverse microradiography (TMR), optical coherence tomography (OCT), scanning electron microscopy (SEM) and confocal laser scanning microscopy (CLSM) have the capabilities to measure subsurface changes to enamel caused by erosion [10,11]. TMR, which is considered the gold standard technique for measuring average mineral loss as a function of depth for carious lesions, has been shown to be capable of measuring erosive lesions [12], albeit after 30 minutes of erosion [13]. TMR requires destructive sample preparation; thin, highly polished sections of enamel are required. SEM has been used mostly to visualise surface topography after exposure to erosion [14]. Cross sectional analysis with SEM is possible through destructive sample preparations like those used in TMR where the sample is cut into sections [15]. One study by Fowler et al [16] used a similar procedure to TMR to quantify mineral loss as function of depth using SEM, showing increases in sensitivity by the greater resolving power attributed to SEM [16]. OCT is a non-destructive method used clinically to assess carious lesions by use of long wavelength light and optical scattering to create 3D images of the lesion [17–19]. OCT has been shown capable of detecting erosive lesions by the intensity of backscattered light as a function of depth accomplished by Chew et al [20], but OCT suffers from limited spatial resolution for reliable use in erosion studies [21].

CLSM is another non-destructive technique able to quantify and visualise erosive lesions. It is capable of high-resolution (sub-micron) images of the microstructure throughout the erosive lesion by optical sectioning. CLSM has been utilised to measure bulk tissue loss and depth of erosive and carious lesions [22,23]. Bulk tissue loss was estimated through height mapping using CLSM [22,24,25], while lesion depth has been typically detected through sectioning of the enamel samples making it a destructive technique [26–28]. It is capable of non-destructively measuring lesion depth as shown by Mia et al [23] using cross sectional images to estimate depth [23]. The area of fluorescence, and total fluorescence, of carious lesions measured by CLSM has been previously shown to correlate well with mineral loss measured by TMR [29,30], showing mineral loss is related to pore space infiltrated by fluorescent dye. CLSM image processing methods have improved over time with increases in computing power allowing for complex 3D images to be quantified for different variables (e.g. volume) using fluorescent dyes, something this paper aims to show.

Typically, erosion is thought to progress through layer by layer removal of the surface, sometimes with little thought given to changes beneath and to the softened surface. A steady state has been proposed where the rate of softening and bulk tissue loss remain constant [31], suggesting the lesion depth is limited. An alternative theory is the lesion continues to grow in depth while bulk tissue loss continues to occur something which can only be determined by subsurface measurements of the enamel. CLSM

is uniquely capable of determining the effect to the subsurface lesion and shedding light on the possible mechanism by which erosion occurs. Thus, the aim of this study is to show erosive lesions created under different conditions are distinguishable by fluorescent volume depth profiles, through the novel application of image processing of fluorescent CLSM images, with a further aim of showing the lesion growth as a function of depth.

2 Methods

2.1 Sample Preparation

The facial surfaces of bovine incisors were polished using P400 paper to give a flat enamel surface, the labial surface was polished using P80 paper until enamel was on one side and dentine the other, with surfaces roughly plano-parallel. The enamel blocks were cut using a water-cooled diamond wafering blade (Well, Walter Ebner, le Locle, 3242, Switzerland) roughly 3 mm in width. The ends were flattened using P400 paper resulting in rectangular blocks ca. 1.0 ± 0.2 cm in length. Enamel blocks were set in 25 mm resin discs with the enamel surface on the outside of the block with 4 parallel blocks per disc. The underside of the block was ground flat with P80 paper and polished by P1200 to optimise subsequent analysis. The enamel sides of the discs were serially polished using P1200, P2500 paper then a 1 µm diamond polish to give a highly polished surface. The thickness of the disc was 6.0 ± 0.5 mm. The discs were sonication for 5 min and rinsed with deionised water before and after. The enamel was stored in 0.2% thymol solution.

2.2 Surface microhardness

Vickers Hardness measurements were carried using a surface microhardness indenter (Struers Duramin 1, Ver.2.01) with a constant Load (1.98 N) and 10 s dwell time. Before analysis the objective lens (40x, NA 0.65) was zero set and calibrated to a known standard (400 kg mm^{-2}) using the test parameters. The samples were tested 6 times for a mean surface hardness value before (SMH_b) and after erosion (SMH_e). Change in hardness (ΔSMH) was calculated by subtracting mean erosion hardness from mean baseline hardness values ($SMH_b - SMH_e = \Delta SMH$).

2.3 Experimental procedure

Twenty randomly selected resin discs (4 enamel blocks per disc, n = 80) were allocated to 10 groups so that mean microhardness values were not significantly different. Each group was acid etched with 0.05 M citric acid (pH 3.8 adjusted with KOH) with and without stirring for time periods of 1, 5, 10, 15, 30 min, using a stirrer bar hot plate (Stuart Hotplate Stirrer SB302) set at ≈150 rpm. Half of each enamel sample was protected by acid resistant tape to preserve a sound enamel surface for subsequent analysis. After acid immersion the enamel samples were rinsed for 10 seconds with deionised water and left to air dry.

2.4 Profilometry

Non-contact 3D profilometry (Scantron, Proscan 2000, sensor S13/1.1) was performed after erosion. The samples were scanned in raster pattern with a 50-micron step in the x and y directions covering the entire sample with a lateral resolution of 25 nm. A sampling rate of 100 Hz was used to average 8 scans. The step height was measured using the dedicated Scantron software (Proscan V2.1.1.15B). The image was levelled by 3-point levelling of the reference surface to account for any unevenness in flatness of the samples. The average height of the data inside a consistent measurement area 10 µm either side of the step formed from erosion was measured. The difference between the eroded and reference zones average height was deemed the step height, which were averaged over 3

measurements per sample. The mean step height collected was determined to be the net bulk tissue loss of the sample.

2.5 Confocal microscopy

The enamel samples were stained with rhodamine B (0.1 mM, pH 8) for 24 h. Staining was performed in a fridge at 8 °C to prevent photobleaching. The samples were then mounted onto a glass slide (No. 1.5) with an immersion oil (Olympus immersion oil Type-F, MOIL-30). The samples were imaged in fluorescence mode by an inverted confocal laser scanning microscope (Olympus Fluo View FV1000, FV10-ASW Software Ver.4.1.1.5) using an oil immersion lens (Zeiss ACHROPLAN, 100x, NA 1.25). A 543 nm laser (HeNe-G/ Helium-Neon gas laser) with intensity of 49 % was used to excite rhodamine B. An emission spectrum was captured between 555 to 655 nm. A scan speed of 10 µs per pixel was used with an image window of 512:512 pixels and a zoom of 2, resulting in a voxel size of 0.124 (x) x 0.124 (y) x 0.600 (z) µm. Gain and offset were kept constant throughout all imaging with adjustment to brightness made by fine-tuning the detector voltage. A pinhole of 246 µm was employed by the software automatically.

2.6 Image Processing

Fiji (Image J, Ver.1.52i) was used to process the images and produce fluorescence volumetric data. The sample image was loaded into Image J as a 12-Bit image. A rolling ball algorithm with pixel size 20 was used to subtract the background and reduce any uneven illumination of the sample. A median filter was applied with pixel radius of 2 to reduce noise while preserving object edges. A local contrast enhancement was performed with block size (10 pixels) increasing the histogram binning. An automatic threshold of 'huang' was used to segment the objects (fluorescent dye) from the background and create a binary image by the stack histogram. The image was then measured for foreground and background pixels/voxels. An area was calculated from the known pixel dimensions and an area fraction as a function of depth was determined for every sample and plotted in Excel.

The area as a function of depth of each sample was aligned by a defined surface and fluorescent area was calculated as a function of depth. Area under the curve analysis was used to provide volumes of fluorescence between each image. The average change in fluorescent volume (ΔFV) was determined by subtracting the volumetric data of a reference image from the data of an eroded image. The data were subsequently averaged and plotted.

2.7 Statistical analysis

2-Way ANOVA was performed in a dedicated statistical package (IBM SPSS, Ver25) along with Tukey post hoc tests to detect significant differences in mean ΔSMH and step heights between erosion time and agitation method ($P<0.05$). Pearson correlations between measured variables were calculated and tested for significance in SPSS ($P<0.01$). Linear regression analyses were performed within Excel.

3 Results

Control images in Figure (1) for both stirred and unstirred solutions show an intact enamel surface with scratches created by the polishing procedure during sample preparation. Acid erosion, for 1 min, led to no distinct visual differences on the surface or orthogonal view for samples exposed to either stirred or unstirred solutions. After 5 and 15 min of erosion, clear damage to the enamel surface was observed for stirred and unstirred solutions, showing a rougher more damaged enamel surface evident from less visible residual scratches from sample preparation. After 30 min of exposure, the surface was highly eroded with increased roughness compared to the reference images. While comparing the orthogonal views a clear increase in the amount of rhodamine B fluorescence (light grey) was observed, indicative of the erosive lesion beneath the surface. More erosive damage to the surface was observed for stirred samples by 5 min, whereas in the orthogonal view a thicker erosive lesion (light grey region) for the stirred sample was observed by 10 min.

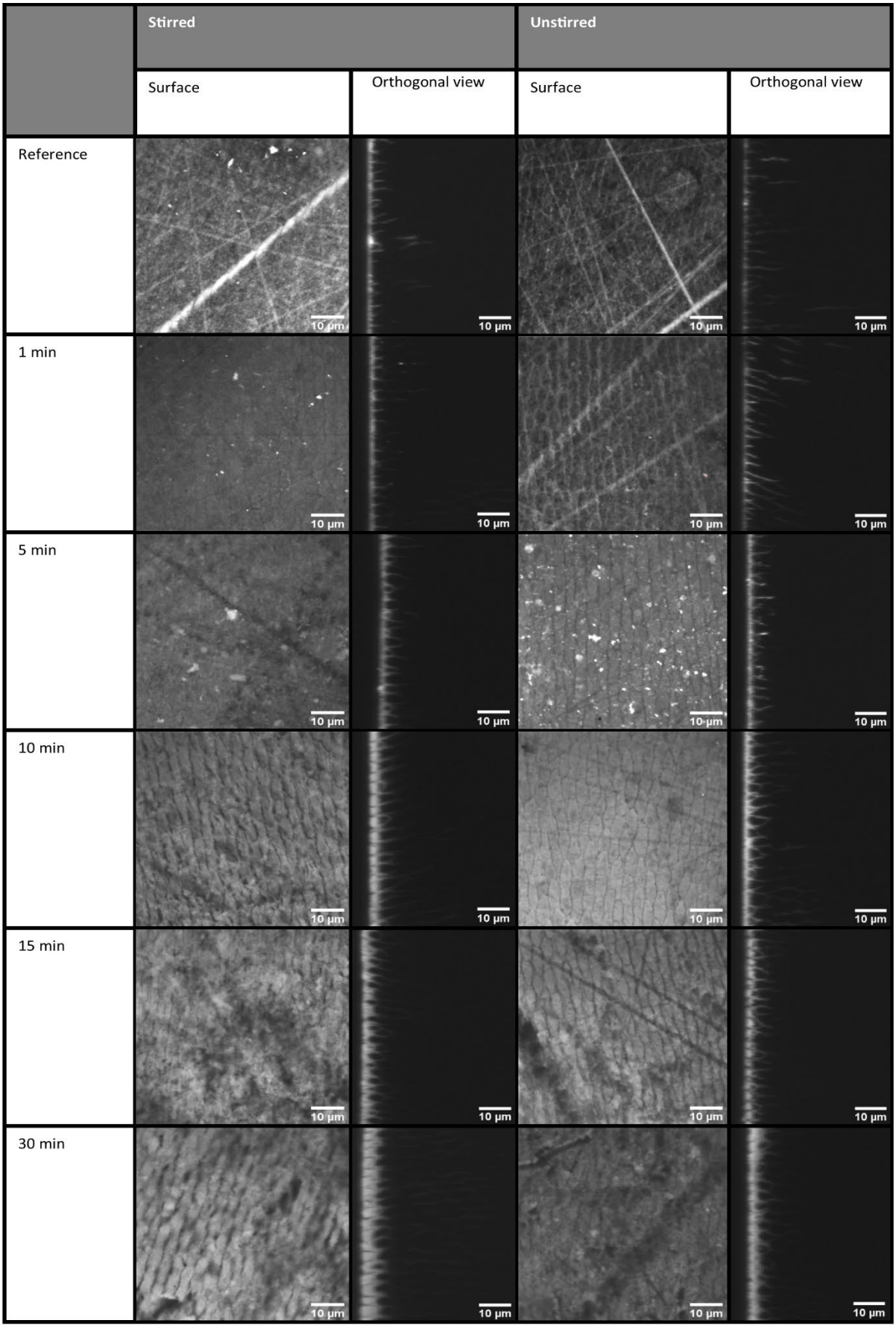

Figure 1: Representative images of rhodamine B-stained bovine enamel captured by CLSM after erosive damage by stirred and unstirred acid solutions for different time periods (t= 0, 1, 5, 15, 30 min).

Increasing duration of acid exposure increased the mean fluorescent volume as a function of depth, reflecting enhanced uptake of rhodamine B dye (Figure (2) a) and b)). All samples exhibited a maximum fluorescent volume (FV) between 75-88 % at the surface (y axis), where dye penetration was greatest, irrespective to the duration of acid exposure or agitation method. Stirred acid solutions show higher FV nearer the surface with increased acid exposure compared to unstirred exposed samples. The erosive lesions were observed to grow in depth as duration of exposure to acid was increased for both stirred and unstirred samples. Higher FV was observed near the surface (to 5 μm) for stirred solutions, whereas for unstirred conditions, FV extended to beyond 10 μm showing a minor elevation of mineral loss with depth.

Changes in fluorescent volume (ΔFV) as a function of depth revealed that increasing the acid exposure duration increased the ΔFV (Figure (2) c) and d)) as a function of depth. The erosive lesions were observed to grow in depth as acid exposure increased as indicated by the elevated ΔFV at greater depths, reflecting enhanced rhodamine B penetration into pore space produce by increasing mineral loss, irrespective of agitation conditions.

Broadly similar patterns were observed in FV and ΔFV for samples exposed to both stirred and unstirred conditions (Figure 2). However, detailed comparison revealed that stirring the acid solution resulted in more mineral loss near the surface (10 μm), as indicated by increases in ΔFV. Mineral loss was shown to be slightly elevated for samples exposed to unstirred conditions at depths beyond 10 microns as indicated by ΔFV.

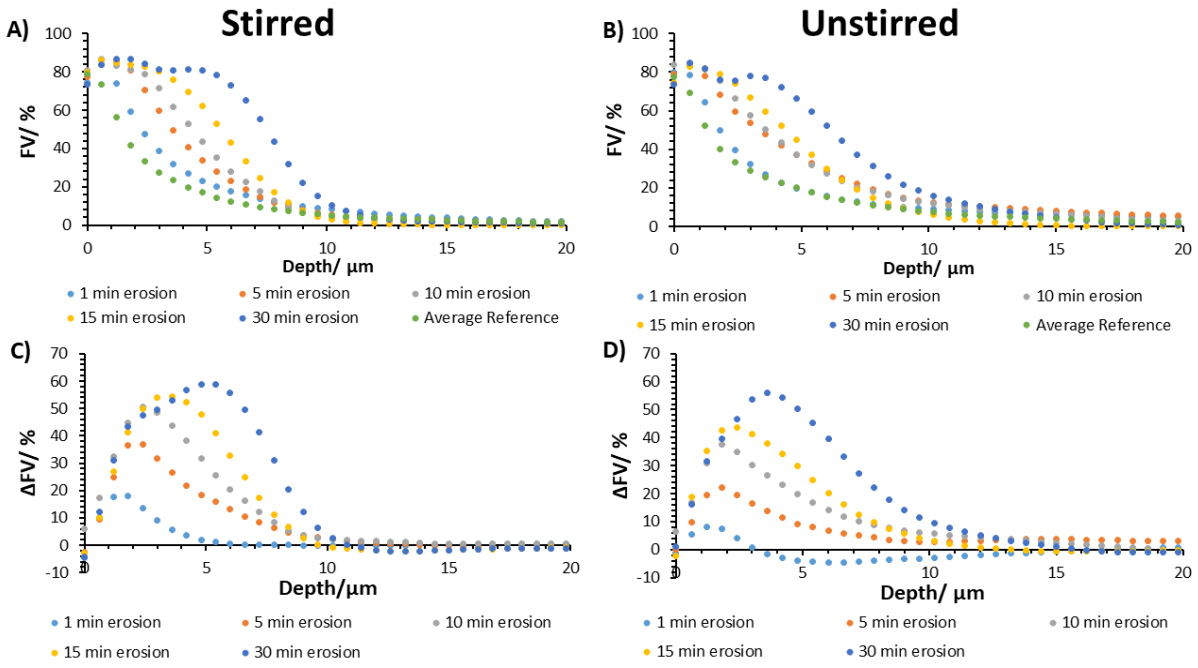

Figure 2: Mean fluorescent volume (FV) as a function of depth of bovine enamel samples exposed to a) stirred and b) unstirred acid solutions for different lengths (t = 0, 1, 5, 10, 15, 30 min). Changes in fluorescent volume (ΔFV) as a function of depth for bovine enamel samples exposed to c) stirred and d) unstirred acid solutions of different lengths (t = 1, 5, 10, 15, 30 min). Error bars were omitted for clarity with an average standard error for FV and ΔFV of ±2.15 and ±2.35 respectively for all groups.

Mean surface microhardness values at baseline were not significantly different between exposure duration and agitation method (P=0.862). After acid exposure all samples had a significant reduction in hardness values (P<0.005). A total reduction in surface microhardness values of 42.6 and 28.4 % after 30 minutes acid exposure of stirred and unstirred solutions respectively. Figure (3) shows the mean change in surface microhardness (ΔSMH) increased with duration of acid exposure for both stirred and unstirred acid conditions. A clear difference in ΔSMH was observed between stirred and unstirred conditions by 10 minutes, with significance difference detected by 15 minutes (P<0.001). The stirred solutions resulted in higher ΔSMH, showing agitation of the acid medium produced more erosive damage. Plateauing of the enamel hardness loss was beginning to occur from 15 to 30 minutes for stirred and unstirred samples.

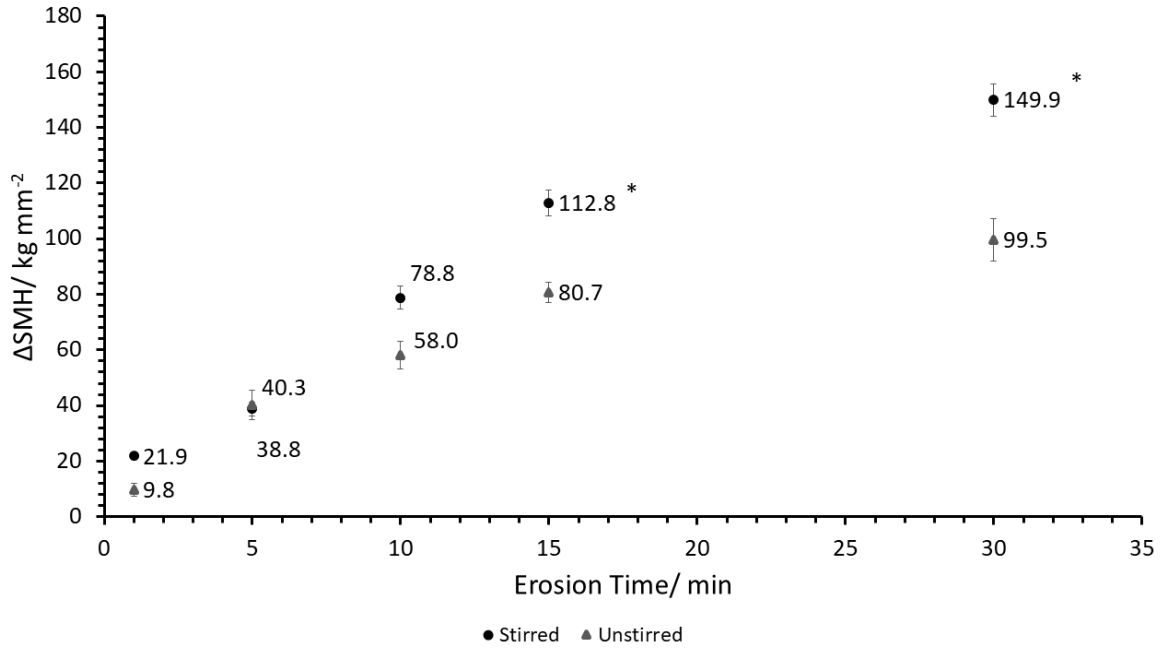

*Figure 3: Mean change in surface microhardness (ΔSMH) from baseline for both stirred and unstirred acid solutions for different times (t = 1, 5, 10, 15, 30 min). Error bars are standard errors. * denotes significant differences between stirred and unstirred acid conditions (P<0.001).*

Average ΔSMH and ΔFV, of the first 12 μm, showed a significant correlation (P<0.01) with Pearson values of 0.854 and 0.830 for stirred and unstirred samples respectively (Table 1).

Table 1: Pearson correlations of the average ΔSMH and ΔFV data of bovine enamel samples exposed to different lengths of stirred and unstirred acid solutions.

	Stirred		**Unstirred**	
Time/ min	**ΔSMH/ kg mm^{-2} (±SE)**	**ΔFV/ % (±SE)**	**ΔSMH/ kg mm^{-2} (±SE)**	**ΔFV/% (±SE)**
1	21.9 (±1.15)a	3.86 (±1.68)a	9.8 (±2.32)a	-1.19 (±2.35)a
5	38.8 (±2.53)a	13.70 (±1.31)b	40.3 (±5.31)b	8.51 (±3.25)a,b
10	78.8 (±4.16)b	20.64 (±1.89)b,c	58.0 (±5.01)b	16.24 (±2.49)b,c
15	112.8 (±4.73)c	23.31 (±1.09)c,d	80.7 (±3.63)c	20.20 (±2.31)c,d
30	149.9 (±5.83)d	31.25 (±3.20)d	99.5 (±7.71)c	29.18 (±2.40)d
	Pearson Value	0.854*	**Pearson Value**	0.830*

*** Denotes significant correlation (P<0.01).**
Different lower-case letters denote significant differences between groups (P<0.05).

Figure 4 shows bulk tissue loss increased with duration of acid exposure as indicated by step height measured by non-contact profilometry. Bulk tissue loss was higher for stirred acid solutions at all-time points. Stirred acid samples lost significantly more bulk tissue than unstirred samples by 10 minutes ($P<0.001$). Linear regression analyses of Figure (4) showed a rate of bulk tissue loss of 0.366 and 0128 µm min^{-1} for stirred and unstirred acid solutions respectively. Linear regression analysis showed a good linear fit of 0.803 for stirred acid exposed samples. Unstirred acid exposed samples showed a lower fit to the linear regression with a R^2 value of 0.624. Deviation away from a linear rate of bulk tissue loss had begun to occur from 15 minutes for unstirred samples. Stirring the solutions resulted in more bulk tissue loss with possible saturation at the surface occurring for unstirred solutions resulting in a deviation from a linear fit.

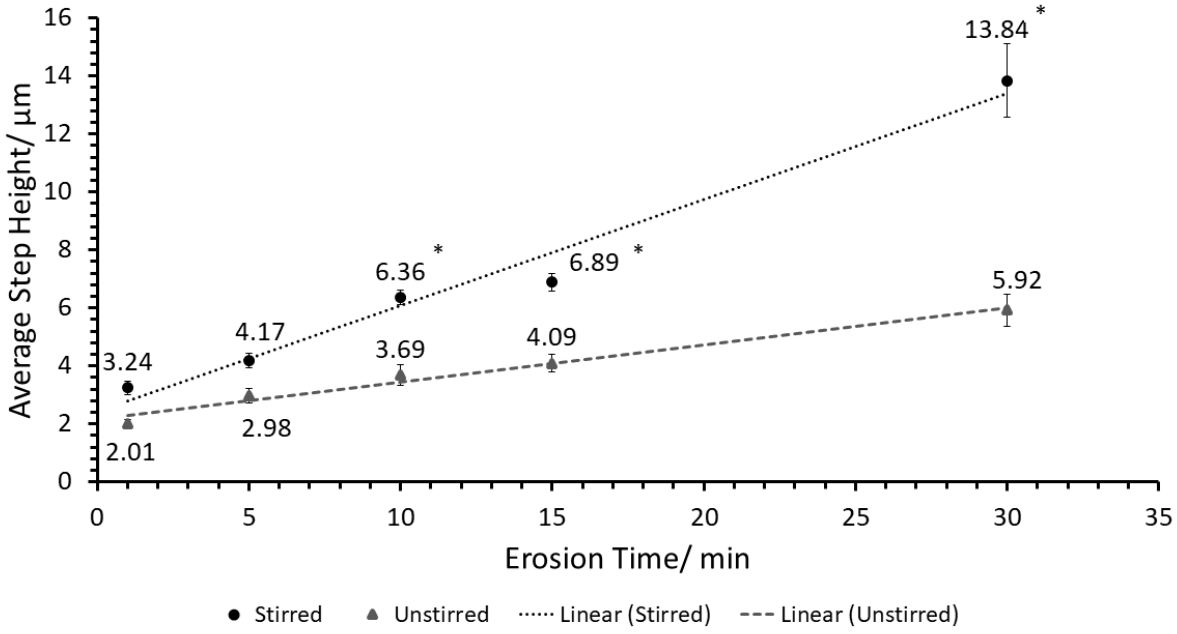

*Figure 4: Average bulk tissue loss from baseline for both stirred and unstirred acid solutions for different times (t= 1, 5, 10, 15, 30 min) measured by non-contact profilometry. Error bars are standard errors. * denotes significant differences between stirred and unstirred acid conditions (P<0.001)*

4 Discussion

The novel approach to image acquisition and processing of CLSM data shown in this study is capable of non-destructive quantification of mineral loss indirectly as a function of depth, through fluorescent dye penetration into pore space. It is also capable of detecting differences between erosive lesions created under different conditions. The sensitivity of this innovative approach is high with the capability of distinguishing differences in depth profiles between 1 and 5 minutes of erosion and between stirred and unstirred samples. Shorter erosive exposure periods (t<1 min) may prove difficult to measure but with an adequately resolved system it should be achievable. The signal detected is specific to rhodamine B by altering the bandpass filter to detect the range of fluorescent light emitted by rhodamine B preventing any auto fluorescence influencing the image acquisition, while also requiring no polarisation.

Citric acid was chosen as the acid medium due to the commonality of this acid within the human diet [32]. Bovine enamel is a widely accepted analogue for human samples [33–38], as it is acquirable in large uniform amounts, is unaffected by human dietary acids, is economic and easier to handle. Small differences in microstructure exist, with bovine enamel having increased porosity, which allows for easier dye penetration, making imaging and processing less complex [36–38]. The use of human samples should be considered for moving forward to more clinically relevant models. Rhodamine B has previously been shown to readily penetrate demineralised enamel [29,39], possibly due to its cationic nature, making it appropriate for use in studies of this type [39,40].

The findings that rates of erosion was greater for stirred solutions compared to unstirred is in agreement with other studies [41–43], presumably due to the prevention of build-up of minerals at the surface, increasing undersaturation of the solution at the near surface (Nernst layer) [44]. This increased rate was also captured non-destructively by CLSM, showing variations in surface topography and pore morphology of the lesion beneath the surface from the same image, something which has previously not been reported. During the erosion process mineral is lost resulting in increases in pore volume, something which has been confirmed from BET isotherms [45], as was observed by CLSM and quantified through image processing. Stirring the acid showed greater mineral loss near the surface by increased pore volume infiltrated with fluorescent dye, which is in agreement with SMH of other studies and with ΔSMH presented here [43].

Interestingly the rate of softening was shown to decrease for both stirred and unstirred solutions after 15 minutes, showing plateauing of hardness loss. This plateauing may point towards a steady state forming with respect to the rate of tissue loss and lesion progression reaching equilibrium, causing softening to remain constant with time as proposed by Lussi et al [31].

The novel application of image processing methodology to CLSM suggested that a steady state had not been reached, with the lesion growing significantly from 15 to 30 minutes acid exposure, for both stirred and unstirred solutions. This finding may be explained by the diffusion of acid into the enamel sub-surface removing mineral preferentially. CLSM also showed that unstirred samples had elevated fluorescent volumes at greater depths (depth >10 microns) meaning the acid was able to diffuse into deeper areas of the enamel to remove preferentially the most soluble material. These findings agree with the bulk tissue loss measurements, which showed the agitation of the acid increased the rate of erosion, by prevention of mineral build-up, which ultimately increases the erosive capacity of the acid. This would allow the unstirred acid to penetrate deeper as observed by the results collected by this novel CLSM image processing method. These findings show that SMH of the surface may not show the entire picture of erosion owing to the limited penetration of the indenter (≈5 μm) [34], meaning anything below this value is unaccounted for. Similar conclusions have been drawn between SMH of

caries lesions upon lamination of the lesion surface [34]. The CLSM data was shown to correlate well with SMH results but this should be taken with care, due to the inherent differences in measurements. Furthermore, the benefit of the CLSM depth profiles of enamel erosive lesions allows for greater understanding of the damage caused below the surface something which SMH or profilometry are not capable off.

Image processing CLSM allowed for both qualitative and quantitative information to be acquired from the same method, which was capable of distinguishing between different erosive lesions created under different conditions. The novel application of image processing to CLSM shows that the erosive lesion is in fact more complex than originally thought, with dynamic changes to pore space which will ultimately alter the characteristics measured by other methods, such as SMH. It has been shown that applying image processing to CLSM images is a viable method for assessing the extent of erosion both visually and quantitively, something which has not been reported before.

Other common methods for measuring erosion are SMH, profilometry, TMR, SEM and OCT which have all been shown to provide a host of benefits and drawbacks which will be discussed [10,46,47].

SMH is a well-established technique and has been used extensively in dental research for erosion and caries studies [48,49]. This method benefits from quick physical measurements to the surface but ultimately only provides information on hardness change, which as detailed above may not show the entire picture regarding erosion [34].

Profilometry is used to measure step height and roughness which is commonly used to assess erosion [22,23]. Profilometry again is only able to provide information regarding changes to the surface much like SMH. An improvement to profilometry has been made to estimate the lesion depth by removal of the lesion through sonication. This improvement creates a destructive technique with no guarantee the erosive lesion was entirely removed [50]. Furthermore, profilometry has been shown to be unable to measure step height changes below 0.5 μm, making subtle changes caused by initial erosion difficult to quantify [51].

TMR is a gold standard method for determining lesion depth, average mineral loss of caries lesions [29,48,52], but has seen limited success for erosive lesions, unless severely eroded ($t > 30$ min) [13] due to sensitivity. TMR involves extensive sample preparation involving sectioning and polishing, which can destroy the surface and render the analysis useless. TMR requires bespoke equipment and extensive experience to acquire reliable data making it difficult to gain access too. Furthermore, TMR does not give prism morphological or surface topographical data.

SEM is typically used to visualise the effects to the enamel surface caused by erosion [15,53]. Sub-surface analysis of prism morphology can be achieved by cross sectioning the enamel sample, a destructive method [16]. Average mineral loss can be determined in a similar manner as TMR as shown by Fowler et al [16] which provided a clear improvement in resolution attributed to the SEM. This method of SEM analysis still suffers from similar problems as TMR namely the destructive nature of the technique and requiring access to bespoke equipment and expertise.

OCT is a non-destructive technique which has been utilised to image erosive and carious lesions [17–19,54]. The use of long wavelength light does not damage the sample, but it is affected by artefacts from reflections and scattering. OCT has also been shown to have a limited depth resolution making it unreliable for imaging erosion as a function of depth as shown by Mylonas et al [21].

While the above techniques have shown varying degrees of success at measuring erosion, they either provide limited or no information regarding the subsurface effects of erosion or require destructive

sample preparation. CLSM circumvents the need for sample preparation, such as sectioning and polishing, allowing for imaging of the surface and subsurface in one go, without damaging the sample and surrounding area. While CLSM has a lower resolution than SEM it is more than adequate to image pore spaces of spaces of 50 – 200 nm in size [55], which allows for dye penetration through the interprismatic/crystallite spaces, which increase in size during erosion [56]. CLSM is therefore capable of imaging micro-porosity of enamel as a function of depth something usually only capable using high resolution X-ray micro-CT, which requires significantly more time and investment to acquire images of similar quality.

The novel application of image processing of CLSM allowed for quantification of fluorescent volume as a function of depth for the first time, showing the extent of erosion beneath the surface. This allows for tracking of the progression of the erosive lesion over time, providing information on the way lesions form. The novel approach allows for new insights into the dental erosion process allowing for a better understanding to be achieved, with multiple variables measured within one technique. A current limitation of CLSM is the imaging of different locations of the same sample for reference and eroded areas, like TMR which assumes the samples would react in the same way.

The use of bespoke equipment like TMR, SEM and OCT make access to these methods difficult, something which CLSM is unaffected by, due to the commonality of the equipment across research institutes. Free access to image processing software (ImageJ) makes this method highly accessible to concomitantly assess mineral loss as a function of depth by fluorescent volume. Image acquisition and processing are quick, making it possible to screen large samples sets more economically, as only fluorescent staining of samples is required. The commonality and free access to CLSM and processing software also increases the comparability across research institutes, allowing for easier comparison of studies.

Use of super resolution microscopy may provide further information on the progression of dental erosion and should be explored for detecting morphological changes to pore spaces created under different erosive conditions. Further development in image processing techniques should allow for greater segmentation of fluorescence from the background, allowing for more accurate measurements to be obtained. Correlation of the parameters used to measure dental erosion by CLSM with mineral loss measured by TMR should be confirmed by experimentation. With this in mind exploration on the ability to measure carious and erosive lesions, in a similar manner to TMR, should be explored to correlate the findings and validate the use of CLSM as an alternative technique. This method of CLSM should be further explored in relation to detecting differences in enamel created under more clinically relevant conditions to explore the potential of this analysis technique.

5 Conclusion

In conclusion, this novel approach to capturing and processing CLSM data, complemented by SMH and non-contact profilometry, presents a new holistic approach to measuring mineral loss as a function of depth of erosive lesions, without complex destructive sample preparation.

References:

[1] J.J. Murray, C.R. Vernazza, R.D. Holmes, Forty years of national surveys: An overview of children's dental health from 1973-2013, BDJ. 219 (2015) 281–285. https://doi.org/10.1038/sj.bdj.2015.723.

[2] J.H. Nunn, P.H. Gordon, A.J. Morris, A. Walker, Dental erosion - changing prevalence? A review of British national childrens' surveys, Int. J. Paediatr. Dent. 13 (2003) 98–105. https://doi.org/10.1046/j.1365-263X.2003.00433.x.

[3] M. Skalsky Jarkander, M. Grindefjord, K. Carlstedt, Dental erosion, prevalence and risk factors among a group of adolescents in Stockholm County, Eur. Arch. Paediatr. Dent. 19 (2018) 23–31. https://doi.org/10.1007/s40368-017-0317-5.

[4] C. Robinson, R.C. Shore, S.J. Brookes, S. Strafford, S.R. Wood, J. Kirkham, The chemistry of enamel caries., Crit. Rev. Oral Biol. Med. 11 (2000) 481–95. https://doi.org/10.1177/10454411000110040601.

[5] R. Moazzez, D. Bartlett, Intrinsic Causes of Erosion, in: A. Lussi, C. Ganss (Eds.), Erosive Tooth Wear From Diagnosis to Ther., 2nd ed., KARGER, Basel, 2014: pp. 180–196. https://doi.org/10.1159/000360369.

[6] T.S. Carvalho, A. Lussi, Susceptibility of Enamel to Initial Erosion in Relation to Tooth Type, Tooth Surface and Enamel Depth, Caries Res. 49 (2015) 109–115. https://doi.org/10.1159/000369104.

[7] R.P. Shellis, J.D.B. Featherstone, A. Lussi, Understanding the Chemistry of Dental Erosion, in: A. Lussi, C. Ganss (Eds.), Monogr. Oral Sci., KARGER, Basel, 2014: pp. 163–179. https://doi.org/10.1159/000359943.

[8] N. Schlueter, L. Neutard, J. Von Hinckeldey, J. Klimek, C. Ganss, Tin and fluoride as anti-erosive agents in enamel and dentine in vitro, Acta Odontol. Scand. 68 (2010) 180–184. https://doi.org/10.3109/00016350903555395.

[9] G.C. De Oliveira, G.P.G. Tereza, A.P. Boteon, B.M. Ferrairo, P.S.P. Gonçalves, T.C. Da Silva, H.M. Honório, D. Rios, Susceptibility of bovine dental enamel with initial erosion lesion to new erosive challenges, PLoS One. 12 (2017) e0182347. https://doi.org/10.1371/journal.pone.0182347.

[10] N. Schlueter, A. Hara, R.P. Shellis, C. Ganss, Methods for the measurement and characterization of erosion in enamel and dentine, Caries Res. 45 (2011) 13–23. https://doi.org/10.1159/000326819.

[11] R.P. Shellis, C. Ganss, Y. Ren, D.T. Zero, A. Lussi, Methodology and Models in Erosion Research: Discussion and Conclusions, Caries Res. 45 (2011) 69–77. https://doi.org/10.1159/000325971.

[12] A.F. Hall, J.P. Sadler, R. Strang, E. de Josselin de Jong, R.H. Foye, S.L. Creanor, Application of transverse microradiography for measurement of mineral loss by acid erosion., Adv. Dent. Res. 11 (1997) 420–5. https://doi.org/10.1177/08959374970110040701.

[13] B.T. Amaechi, S.M. Higham, W.M. Edgar, Use of Transverse Microradiography to Quantify Mineral Loss by Erosion in Bovine Enamel, Caries Res. 32 (1998) 351–356. https://doi.org/10.1159/000016471.

[14] J.H. Min, H.K. Kwon, B.I. Kim, The addition of nano-sized hydroxyapatite to a sports drink to inhibit dental erosion - In vitro study using bovine enamel, J. Dent. 39 (2011) 629–635.

https://doi.org/10.1016/j.jdent.2011.07.001.

[15] N. Schlueter, M. Hardt, A. Lussi, F. Engelmann, J. Klimek, C. Ganss, Tin-containing fluoride solutions as anti-erosive agents in enamel: An in vitro tin-uptake, tissue-loss, and scanning electron micrograph study, Eur. J. Oral Sci. 117 (2009) 427–434. https://doi.org/10.1111/j.1600-0722.2009.00647.x.

[16] C. Fowler, R.J.M. Lynch, D. Shingler, D. Walsh, C. Carson, A. Neale, R.J. Willson, A. Brown, A novel electron-microscopic method for measurement of mineral content in enamel lesions, Arch. Oral Biol. 94 (2018) 10–15. https://doi.org/10.1016/j.archoralbio.2018.06.013.

[17] H.-M. Ku, B.-R. Kim, S.-M. Kang, J.-H. Chung, H.-K. Kwon, B.-I. Kim, Detection of early changes in caries lesion using QLF-D and OCT, J. Korean Acad. Oral Heal. 38 (2014) 10–16. https://doi.org/10.11149/jkaoh.2014.38.1.10.

[18] J. Gomez, C. Zakian, S. Salsone, S.C.S. Pinto, A. Taylor, I.A. Pretty, R. Ellwood, In vitro performance of different methods in detecting occlusal caries lesions, J. Dent. 41 (2013) 180–186. https://doi.org/10.1016/j.jdent.2012.11.003.

[19] M. Machoy, J. Seeliger, L. Szyszka-Sommerfeld, R. Koprowski, T. Gedrange, K. Woźniak, The Use of Optical Coherence Tomography in Dental Diagnostics: A State-of-the-Art Review, J. Healthc. Eng. 2017 (2017) 1–31. https://doi.org/10.1155/2017/7560645.

[20] H.P. Chew, C.M. Zakian, I.A. Pretty, R.P. Ellwood, Measuring initial enamel erosion with quantitative light-induced fluorescence and optical coherence tomography: An in vitro validation study, Caries Res. 48 (2014) 254–262. https://doi.org/10.1159/000354411.

[21] P. Mylonas, R.S.S. Austin, R. Moazzez, A. Joiner, D.W.W. Bartlett, In vitro evaluation of the early erosive lesion in polished and natural human enamel, Dent. Mater. 34 (2018) 1391–1400. https://doi.org/10.1016/j.dental.2018.06.018.

[22] R.S. Austin, C.L. Giusca, G. Macaulay, R. Moazzez, D.W. Bartlett, Confocal laser scanning microscopy and area-scale analysis used to quantify enamel surface textural changes from citric acid demineralization and salivary remineralization in vitro, Dent. Mater. 32 (2016) 278–284. https://doi.org/10.1016/j.dental.2015.11.016.

[23] A.M.A. Maia, C. Longbottom, A.S.L. Gomes, J.M. Girkin, Enamel erosion and prevention efficacy characterized by confocal laser scanning microscope, Microsc. Res. Tech. 77 (2014) 439–445. https://doi.org/10.1002/jemt.22364.

[24] A.M. Paepegaey, M.L. Barker, D.W. Bartlett, M. Mistry, N.X. West, N. Hellin, L.J. Brown, P.G. Bellamy, Measuring enamel erosion: A comparative study of contact profilometry, non-contact profilometry and confocal laser scanning microscopy, Dent. Mater. 29 (2013) 1265–1272. https://doi.org/10.1016/j.dental.2013.09.015.

[25] Y.L. Wang, C.C. Chang, C.W. Chi, H.H. Chang, Y.C. Chiang, Y.C. Chuang, H.H. Chang, G.F. Huang, Y.S. Liao, C.P. Lin, Erosive potential of soft drinks on human enamel: An invitro study, J. Formos. Med. Assoc. 113 (2014) 850–856. https://doi.org/10.1016/j.jfma.2014.06.002.

[26] P. Somasundaram, L. Mandke, N. Vimala, Protective potential of casein phosphopeptide amorphous calcium phosphate containing paste on enamel surfaces, J. Conserv. Dent. 16 (2013) 152–156. https://doi.org/10.4103/0972-0707.108199.

[27] K. Chokshi, A. Chokshi, S. Konde, S.R. Shetty, K.N. Chandra, S. Jana, S. Mhambrey, S. Thakur, An in vitro comparative evaluation of three remineralizing agents using confocal microscopy, J. Clin. Diagnostic Res. 10 (2016) ZC39–ZC42. https://doi.org/10.7860/JCDR/2016/18191.7984.

[28] Y. Zhou, K. Matin, Y. Shimada, Y. Sumi, J. Tagami, Evaluation of resin infiltration on demineralized root surface: An in vitro study, Dent. Mater. J. 36 (2017) 195–204. https://doi.org/10.4012/dmj.2016-229.

[29] M. Fontana, Y. Li, P. Dunipace, T.W. Noblitt, G. Fischer, B.P. Katz, G.K. Stookey, Measurement of enamel demineralization using microradiography and confocal microscopy, Caries Res. 30 (1996) 317–325. https://doi.org/10.1159/000262337.

[30] C. González-Cabezas, M. Fontana, A.J. Dunipace, Y. Li, G.M. Fischer, H.M. Proskin, G.K. Stookey, Measurement of enamel remineralization using microradiography and confocal microscopy: a correlational study, Caries Res. 32 (1998) 385–392. https://doi.org/10.1159/000016475.

[31] A. Lussi, N. Schlueter, E. Rakhmatullina, C. Ganss, Dental erosion – an overview with emphasis on chemical and histopathological aspects, Caries Res. 45 (2011) 2–12. https://doi.org/10.1159/000325915.

[32] J.A. Hughes, N.X. West, D.M. Parker, M.H. Van Den Braak, M. Addy, Effects of pH and concentration of citric, malic and lactic acids on enamel, in vitro, J. Dent. 28 (2000) 147–152. https://doi.org/10.1016/S0300-5712(99)00060-3.

[33] J. de D. Teruel, A. Alcolea, A. Hernández, A.J.O. Ruiz, Comparison of chemical composition of enamel and dentine in human, bovine, porcine and ovine teeth, Arch. Oral Biol. 60 (2015) 768–775. https://doi.org/10.1016/j.archoralbio.2015.01.014.

[34] F. Lippert, R.J.M. Lynch, Comparison of Knoop and Vickers surface microhardness and transverse microradiography for the study of early caries lesion formation in human and bovine enamel, Arch. Oral Biol. 59 (2014) 704–710. https://doi.org/10.1016/j.archoralbio.2014.04.005.

[35] A.J. White, C. Yorath, V. Ten Hengel, S.D. Leary, M.-C.D.N.J.M. Huysmans, M.E. Barbour, Human and bovine enamel erosion under 'single-drink' conditions, Eur. J. Oral Sci. 118 (2010) 604–609. https://doi.org/10.1111/j.1600-0722.2010.00779.x.

[36] P. Laurance-Young, L. Bozec, L. Gracia, G. Rees, F. Lippert, R.J.M. Lynch, J.C. Knowles, A review of the structure of human and bovine dental hard tissues and their physicochemical behaviour in relation to erosive challenge and remineralisation, J. Dent. 39 (2011) 266–272. https://doi.org/10.1016/j.jdent.2011.01.008.

[37] A.J. Ortiz-Ruiz, J. de D. Teruel-Fernández, L.A. Alcolea-Rubio, A. Hernández-Fernández, Y. Martínez-Beneyto, F. Gispert-Guirado, Structural differences in enamel and dentin in human, bovine, porcine, and ovine teeth, Ann. Anat. 218 (2018) 7–17. https://doi.org/10.1016/j.aanat.2017.12.012.

[38] J. Arends, W.L. Jongebloed, Crystallites dimensions of enamel., J. Biol. Buccale. 6 (1978) 161–171.

[39] J. Canning, G. Huyang, M. Ma, A. Beavis, D. Bishop, K. Cook, A. McDonagh, D. Shi, G.-D. Peng, M. Crossley, Percolation Diffusion into Self-Assembled Mesoporous Silica Microfibres, Nanomaterials. 4 (2014) 157–174. https://doi.org/10.3390/nano4010157.

[40] S.R. Kwon, P.W. Wertz, Y. Li, D.C.N. Chan, Penetration pattern of rhodamine dyes into enamel and dentin: Confocal laser microscopy observation, Int. J. Cosmet. Sci. 34 (2012) 97–101. https://doi.org/10.1111/j.1468-2494.2011.00688.x.

[41] M. Eisenburger, M. Addy, Influence of liquid temperature and flow rate on enamel erosion and surface softening, J. Oral Rehabil. 30 (2003) 1076–1080. https://doi.org/10.1046/j.1365-

2842.2003.01193.x.

[42] R.P. Shellis, M. Finke, M. Eisenburger, D.M. Parker, M. Addy, Relationship between enamel erosion and liquid flow rate, Eur. J. Oral Sci. 113 (2005) 232–238. https://doi.org/10.1111/j.1600-0722.2005.00210.x.

[43] D.W. El Assal, A.M. Saafan, D.H. Moustafa, M.A. Al-Sayed, The effect of combining laser and nanohydroxy-apatite on the surface properties of enamel with initial defects, J. Clin. Exp. Dent. 10 (2018) 425–430. https://doi.org/10.4317/jced.54371.

[44] A. Lussi, T.S. Carvalho, Erosive Tooth Wear: A Multifactorial Condition of Growing Concern and Increasing Knowledge, in: A. Lussi, C. Ganss (Eds.), Erosive Tooth Wear From Diagnosis to Ther., 2nd ed., KARGER, Basel, 2014: pp. 1–15. https://doi.org/10.1159/000360380.

[45] T.T. Nguyen, A. Miller, M.F. Orellana, Characterization of the porosity of human dental enamel and shear bond strength in vitro after variable etch times: initial findings using the BET Method, Angle Orthod. 81 (2011) 707–715. https://doi.org/10.2319/083010-506.1.

[46] M. Joshi, Techniques to Evaluate Dental Erosion: A Systematic Review of Literature, J. Clin. DIAGNOSTIC Res. (2016). https://doi.org/10.7860/JCDR/2016/17996.8634.

[47] T. Attin, F.J. Wegehaupt, Methods for Assessment of Dental Erosion, in: A. Lussi, C. Ganss (Eds.), Erosive Tooth Wear From Diagnosis to Ther., 2nd ed., KARGER, Basel, 2014: pp. 123–142. https://doi.org/10.1159/000360355.

[48] J.D.B. Featherstone, J.M. Ten Cate, M. Shariati, J. Arends, Comparison of artificial caries-like lesions by quantitative microradiography and microhardness profiles, Caries Res. 17 (1983) 385–391. https://doi.org/10.1159/000260692.

[49] F. Lippert, K. Juthani, Fluoride dose-response of human and bovine enamel artificial caries lesions under pH-cycling conditions, Clin. Oral Investig. 19 (2015) 1947–1954. https://doi.org/10.1007/s00784-015-1436-1.

[50] M. Eisenburger, J. Hughes, N.X. West, K.D. Jandt, M. Addy, Ultrasonication as a Method to Study Enamel Demineralisation during Acid Erosion, Caries Res. 34 (2000) 289–294. https://doi.org/10.1159/000016604.

[51] F. Mullan, D. Bartlett, R.S. Austin, Measurement uncertainty associated with chromatic confocal profilometry for 3D surface texture characterization of natural human enamel, Dent. Mater. 33 (2017) e273–e281. https://doi.org/10.1016/j.dental.2017.04.004.

[52] R.J. Wierichs, H. Zelck, C.E. Doerfer, P. Appel, S. Paris, M. Esteves-Oliveira, H. Meyer-Lueckel, Effects of dentifrices differing in fluoride compounds on artificial enamel caries lesions in vitro, Odontology. (2016) 1–10. https://doi.org/10.1007/s10266-016-0233-x.

[53] L. Levrini, G. Di Benedetto, M. Raspanti, Dental wear: A scanning electron microscope study, Biomed Res. Int. 2014 (2014) 1–7. https://doi.org/10.1155/2014/340425.

[54] C.H. Wilder-Smith, P. Wilder-Smith, H. Kawakami-Wong, J. Voronets, K. Osann, A. Lussi, Quantification of dental erosions in patients with GERD using optical coherence tomography before and after double-blind, randomized treatment with esomeprazole or placebo, Am. J. Gastroenterol. 104 (2009) 2788–2795. https://doi.org/10.1038/ajg.2009.441.

[55] H. Deyhle, S.N. White, O. Bunk, F. Beckmann, B. Müller, Nanostructure of carious tooth enamel lesion., Acta Biomater. 10 (2014) 355–364. https://doi.org/10.1016/j.actbio.2013.08.024.

[56] A.L.M. Ubaldini, M.L. Baesso, A. Medina Neto, F. Sato, A.C. Bento, R.C. Pascotto, Hydrogen

peroxide diffusion dynamics in dental tissues., J. Dent. Res. 92 (2013) 661–665. https://doi.org/10.1177/0022034513488893.

List of Figure & Table Captions:

Figure 1: Representative images of rhodamine B-stained bovine enamel captured by CLSM after erosive damage by stirred and unstirred acid solutions for different time periods (t= 0, 1, 5, 15, 30 min).

Figure 2: Mean fluorescent volume (FV) as a function of depth of bovine enamel samples exposed to a) stirred and b) unstirred acid solutions for different lengths (t = 0, 1, 5, 10, 15, 30 min). Changes in fluorescent volume (ΔFV) as a function of depth for bovine enamel samples exposed to c) stirred and d) unstirred acid solutions of different lengths (t = 1, 5, 10, 15, 30 min). Error bars were omitted for clarity with an average standard error for FV and ΔFV of ±2.15 and ±2.35 respectively for all groups.

Figure 3: Mean change in surface microhardness (ΔSMH) from baseline for both stirred and unstirred acid solutions for different times (t = 1, 5, 10, 15, 30 min). Error bars are standard errors. * denotes significant differences between stirred and unstirred acid conditions ($P<0.001$).

Table 1: Pearson correlations of the average ΔSMH and ΔFV data of bovine enamel samples exposed to different lengths of stirred and unstirred acid solutions.

Figure 5: Average bulk tissue loss from baseline for both stirred and unstirred acid solutions for different times (t= 1, 5, 10, 15, 30 min) measured by non-contact profilometry. Error bars are standard errors. * denotes significant differences between stirred and unstirred acid conditions ($P<0.001$)